JOURNAL OF GEOPHYSICAL RESEARCH, VOL. 111, A11102, doi:10.1029/2006JA011901, 2006

Magnetohydrodynamic simulation of the interaction between interplanetary strong shock and magnetic cloud and its consequent geoeffectiveness: 2. Oblique collision

Ming Xiong,[1] Huinan Zheng,[1] Yuming Wang,[1] and Shui Wang[1]

Received 7 June 2006; revised 20 July 2006; accepted 22 August 2006; published 9 November 2006.

[1] Numerical studies of the interplanetary "shock overtaking magnetic cloud (MC)" event are continued by a 2.5-dimensional magnetohydrodynamic (MHD) model in heliospheric meridional plane. Interplanetary direct collision (DC)/oblique collision (OC) between an MC and a shock results from their same/different initial propagation orientations. For radially erupted MC and shock in solar corona, the orientations are only determined respectively by their heliographic locations. OC is investigated in contrast with the results in DC (Xiong, 2006). The shock front behaves as a smooth arc. The cannibalized part of MC is highly compressed by the shock front along its normal. As the shock propagates gradually into the preceding MC body, the most violent interaction is transferred sideways with an accompanying significant narrowing of the MC's angular width. The opposite deflections of MC body and shock aphelion in OC occur simultaneously through the process of the shock penetrating the MC. After the shock's passage, the MC is restored to its oblate morphology. With the decrease of MC-shock commencement interval, the shock front at 1 AU traverses MC body and is responsible for the same change trend of the latitude of the greatest geoeffectiveness of MC-shock compound. Regardless of shock orientation, shock penetration location regarding the maximum geoeffectiveness is right at MC core on the condition of very strong shock intensity. An appropriate angular difference between the initial eruption of an MC and an overtaking shock leads to the maximum deflection of the MC body. The larger the shock intensity is, the greater is the deflection angle. The interaction of MCs with other disturbances could be a cause of deflected propagation of interplanetary coronal mass ejection (ICME).

Citation: Xiong, M., H. Zheng, Y. Wang, and S. Wang (2006), Magnetohydrodynamic simulation of the interaction between interplanetary strong shock and magnetic cloud and its consequent geoeffectiveness: 2. Oblique collision, *J. Geophys. Res.*, *111*, A11102, doi:10.1029/2006JA011901.

1. Introduction

[2] Interplanetary (IP) space is permeated by highly fluctuating solar wind with magnetic field frozen in its plasma [*Parker*, 1963]. The relatively quiet equilibrium of IP space is frequently interrupted by the solar disturbances, especially during solar maximum. Giant clouds of ionized gas with magnetic flux of 10^{23} maxwell and plasma mass of 10^{16} g, called coronal mass ejection (CME), are regularly emitted from the Sun [*Gosling*, 1990; *Webb et al.*, 1994]. IP CME (ICME) generally causes strong perturbation in the space environment as it passes by. Several models have already been applied in space weather forecasting, such as (1) HAF (Hakamada-Akasofu-Fry) [*Fry et al.*, 2001, 2005]; (2) STOA (Shock Time of Arrival) [*Smart and Shea*, 1985]; (3) ISPM (Interplanetary Shock Propagation Model) [*Smith and Dryer*, 1990]; (4) an ensemble of HAF, STOA, and ISPM models [*Dryer et al.*, 2001, 2004]; (5) SWMF (Space Weather Modeling Framework) [*Groth et al.*, 2000; *Gombosi et al.*, 2001; *Toth et al.*, 2005]; (6) HHMS (Hybrid Heliospheric Modeling System) [*Detman et al.*, 2006]; and so on. Great challenges are still faced to improve the prediction performance of space weather to satisfy the ever-increasing demands from human civilization [*Baker*, 2002].

[3] Magnetic clouds (MCs) are an important subset of ICMEs, whose fraction decreases from ~100% (though with low statistics) at solar minimum to ~15% at solar maximum [*Richardson and Cane*, 2004, 2005]. Identified by their characteristics including enhanced magnetic field, large and smooth rotation of magnetic field and low proton temperature [*Burlaga et al.*, 1981], MCs have been the subject of increasingly intense study. The MCs with long interval of large southward magnetic field B_s are widely considered to be the major IP origin of moderate to intense geomagnetic storms,

[1]Chinese Academy of Sciences Key Laboratory for Basic Plasma Physics, School of Earth and Space Sciences, University of Science and Technology of China, Anhui, China.

0148-0227/06/2006JA011901$09.00

especially during the solar maximum [*Tsurutani et al.*, 1988; *Gosling et al.*, 1991; *Gonzalez et al.*, 1999] and hence play a crucial role in space weather prediction. An MC should probably be a curved loop-like structure with its feet connecting to the solar surface [*Larson et al.*, 1997]. The force-free magnetic flux rope models have been proven to be very valuable to interpret in situ observations of MCs [*Lundquist*, 1950; *Goldstein*, 1983; *Burlaga*, 1988; *Farrugia et al.*, 1993]. For the study of evolution of an individual MC during its antisunward propagation, many sophisticated models are developed based on these initial flux rope models: (1) Analytical models [*Osherovich et al.*, 1993a, 1993b, 1995; *Hidalgo*, 2003, 2005]; (2) Kinematic models [*Riley and Crooker*, 2004; *Owens et al.*, 2006]; (3) Numerical models [*Vandas et al.*, 1995, 1996, 1997, 2002; *Groth et al.*, 2000; *Odstrcil et al.*, 2002; *Schmidt and Cargill*, 2003; *Manchester et al.*, 2004a, 2004b]. Especially numerical simulations in (3) on a single MC have been exhaustive under the condition of various magnetic field strengths, axis orientations, and speeds.

[4] ICME is not an absolutely self-isolated entity during IP propagation. It may interact with other solar transients (e.g., shock, ejecta) and heterogenous medium (e.g., corotating interacting region). With less defined characteristics, some IP complex structures are reported recently, such as complex ejecta [*Burlaga et al.*, 2002], multiple MCs [*Wang et al.*, 2002a, 2003a], shock-penetrated MC [*Wang et al.*, 2003b; *Berdichevsky et al.*, 2005], non-pressure-balanced "MC boundary layer" associated with magnetic reconnection [*Wei et al.*, 2003, 2006], ICME compressed by the following high-speed stream [*Dal Lago et al.*, 2006], and so on. Dynamical response and ensuing geoeffectiveness of these structures are directly associated with the interaction during their formation and evolution. Numerical simulations have been applied to study most of the complex structures: e.g., the interaction of a shock wave with an MC [*Vandas et al.*, 1997; *Odstrcil et al.*, 2003; *Xiong et al.*, 2006], and the interaction of two MCs [*Odstrcil et al.*, 2003; *Gonzalez-Esparza et al.*, 2004; *Lugaz et al.*, 2005; *Wang et al.*, 2005].

[5] The observed "shock overtaking MC" events substantiate the likelihood of strong shock propagation in low β medium of MC plasma and therefore present a very interesting topic in IP dynamics. The evolution stages of MC-shock interaction within 1 AU are determined by MC and shock commencement interval in solar corona. They can be assorted into two categories: (1) shock still in MC (e.g., 3–6 October 2000 and 5–7 November 2001 events [*Wang et al.*, 2003b]); (2) shock ahead of MC after completely penetrating it (e.g., 20–21 March 2003 event [*Berdichevsky et al.*, 2005]). The idea that shock compression of the preexisting southward magnetic component can increase geoeffectiveness of the corresponding B_s event has been proved in data analyses [*Wang et al.*, 2003d]. Particularly, MC-shock compounds in category (1) cause highly intense geomagnetic storms [*Wang et al.*, 2003b, 2003c; *Xiong et al.*, 2006]. Furthermore, the geoeffectiveness variance of MC-shock compound with respect to the increasing depth of a shock entering a preceding MC was investigated in our previous study [*Xiong et al.*, 2006, hereinafter referred to as paper 1]. Both MC core and shock nose are radially erupted along heliospheric current sheet (HCS) in paper 1; however, the above-mentioned specific MC-shock events [*Wang et al.*, 2003b; *Berdichevsky et al.*, 2005] were all identified such that the shock flank sweeps the preceding MC body. IP direct collision (DC)/oblique collision (OC) between an MC and a shock results from their same/different initial propagation orientation. For radially erupted MC and shock in solar corona, the orientations are only determined by the heliographic locations of MC core and shock nose, respectively. Because the probability of MC core and shock nose radially launching from the same heliographic location is very rare and shock front extends over a wide angular span in IP medium, it is meaningful to study the role of shock orientation relative to a preceding MC propagation. DC in paper 1 is here modified to be OC for MC-shock interaction. The shock in DC/OC is correspondingly named as "central"/"noncentral" shock. Moreover, DC/OC is likely to be the IP interaction of two radially propagating disturbances from the same/different solar activity regions.

[6] Section 2 presents a brief description of numerical magnetohydrodynamic (MHD) model. Section 3 discusses the dynamical evolution of MC-shock OC. Section 4 analyzes the ensuing geoeffectiveness of MC-shock compound. Section 5 describes the dependence of shock-induced MC deflection on shock orientation and intensity. Section 6 summaries the conclusions.

2. Numerical MHD Model

[7] The detailed description of the numerical model, including numerical scheme, computational mesh layout, prescription of the ambient solar wind and preceding MC, is given in paper 1. Only the shock introduction among input parameters of numerical model is modified to simulate OC of MC-shock interaction in contrast with DC in paper 1.

[8] An incidental fast shock, which is radially launched from the inner boundary, is prescribed by several parameters: its emergence time t_{s0}, the latitude of its nose θ_{sc}, the latitudinal width of its flank $\Delta\theta_s$, the maximum shock speed within its front v_s, the duration of growth, maintenance, and recovery phases (t_{s1}, t_{s2}, t_{s3}). Some parameters are fixed in all simulation cases of paper 1 and here, i.e., $\Delta\theta_s = 6°$, $t_{s1} = 0.3$ hours, $t_{s2} = 1$ hour, $t_{s3} = 0.3$ hours. The remaining parameters (t_{s0}, θ_{sc}, v_s) are independently chosen to mimic different conditions of IP MC-shock interaction. Here t_{s0} is used to separate the MC and shock initialization in time for reproducing different evolutionary stages of MC-shock compound at 1 AU and θ_{sc} designates emergence orientation of shock nose relative to previous MC propagation. Since the preceding MC emerges from the heliospheric equator, $\theta_{sc} = 0°$ and $\theta_{sc} \neq 0°$, corresponding to the introduction of "central" and "noncentral" shock, determine MC-shock DC and OC in IP space respectively. Here v_s describes the intensity of MC-shock interaction to some extent. All introduced shocks in our simulation are strong enough to be faster than the local magnetosonic speed at all time and therefore to prevent weak shock dissipation in MC medium.

3. Dynamics of MC-Shock Interaction

[9] All 50 simulation cases are assorted into five groups in Table 1. Groups of individual MC (IM), direct collision (DC), oblique collision (OC), shock orientation dependence (SOD), and shock intensity dependence (SID) are studied, respectively, where Groups IM and DC have been addressed in

Table 1. Assortment of Simulation Cases of Individual Magnetic Cloud (MC) and MC-Shock Interaction

Group	Case	v_s, km/s	θ_{sc}, deg	t_{s0}, hour	Comment
IM	A	-	-	-	Individual MC
DC	B_1, C_1, D_1, E_1, F_1, G_1, H_1, I_1, J_1, K_1, L_1, M_1, N_1, O_1, P_1, Q_1, R_1	1630	0	41, 10, 60, 50, 48, 46, 44, 38, 35, 32, 29, 26, 23, 20, 15, 6, 3	Direct Collision
OC	B_2, C_2, D_2, E_2, F_2, G_2, H_2, I_2, J_2, K_2, L_2, M_2, N_2, O_2, P_2, Q_2, R_2	1630	10	41, 10, 60, 50, 48, 46, 44, 38, 35, 32, 29, 26, 23, 20, 15, 6, 3	Oblique Collision
SOD	P_1, a, P_2, b, c, d, e, f, g	1630	0, 5, 10, 15, 20, 25, 30, 40, 45	10	Shock Orientation Dependence
SID	h, i, P_2, j, k, l, m, n, o	947, 1226, 1402, 1630, 1773, 1997, 2314, 2686, 3173	10	10	Shock Intensity Dependence

detail in paper 1. Case P_1 is shared by Groups DC and SOD, and Case P_2 is shared by Groups OC, SOD, and SID. With the identical v_s of 1630 kms^{-1} and variable t_{s0} from 3 hours to 41 hours, Groups DC and OC only differ in θ_{sc} for comparative study. By modifying θ_{sc} from 0° to 10°, "central" shock in DC is directed to be "noncentral" one in OC. Further, the parametric studies of θ_{sc} from 0° to 45° in Group SOD and v_s from 947 km s^{-1} to 3173 km s^{-1} in Group SID are explored as a supplement to Groups DC and OC. Cases B_1 and B_2 with t_{s0} = 41 hours, and Cases C_1 and C_2 with t_{s0} = 10 hours are typical examples of MC-shock interaction in categories 1 and 2 referred in section 1.

3.1. Case B_2

[10] The process of MC-shock interaction of Case B_2 is visualized in Figure 1. Under each image are two corresponding radial profiles by cutting right through 0° (noted by Lat. = 0°) and southern 4.5° (white dashed lines in the images, noted by Lat. = 4.5°S) away from the equator. The magnitude of magnetic field in radial profile is given by subtracting its corresponding initial value of ambient equilibrium. The body of MC is identified to be enclosed by a white solid line in the images and between two dotted lines in attached profiles. Magnetic field configuration is superimposed upon the images. The incidental shock aphelion arrives at $90R_s$ (along Lat. = 4.5°S) in 50.4 hours meanwhile the MC core arrives at $160R_s$ (along Lat. = 0°), shown in Figures 1a, 1d, and 1g. Impending collision can be pregnant from large radial speed difference between the preceding MC and the following shock, as indicated by radial bulk flow speed v_r of 830 km s^{-1} at shock front and 540 km s^{-1} at MC head from the profile of Lat. = 4.5°S (Figure 1d). Though the latitudinal span of its flank is 6° initially at inner boundary, the shock extends up to 40° quickly due to its very strong intensity, until it emerges into IP medium completely. The traverse of shock front across the equator leads to significant HCS warping seen clearly in Figure 1b, which is consistent with previous results [*Smith et al.*, 1998; *Hu and Jia*, 2001]. As shock emergence orientation is redirected, the morphology of IP shock changes from a concave (Figure 3e in paper 1) to a smooth arc (Figure 1e here). As a result, MC-shock interaction consequently changes from DC to OC. The shock just catches up with the inner boundary of MC at 66.9 hours (Figures 1b, 1e, and 1h). Owing to strong magnetic field and low β plasma, the radial characteristic speed of fast mode wave c_f of the MC is abnormally high at 1 AU with 200 km s^{-1} in maximum at MC core and 100 km s^{-1} in minimum at MC boundary. The rare chance of shock survival in an MC medium explains why only a few "shock overtaking MC" events are observed in IP space. Across the tangent point between inner MC boundary and shock front exists a quite sharp slope of v_r, as clearly seen along Lat. = 4.5°S. MC-shock interaction begins from this tangent point at 66.9 hours. Once a slow MC is within the very large latitudinal span of the overtaking shock front, it will be swept by the shock and, from then on, the evolution of MC and shock will be coupled with each other. The overwhelming shock significantly distorts MC morphology at 85.4 hours (Figures 1c, 1f, and 1i). Namely, the originally curved magnetic field lines become very flat. The collision is more violent along Lat. = 4.5°S. A sharp discontinuity is conspicuously formed in the rear part of MC with $B - B|_{t=0}$ = 25 nT, v_r = 620 km s^{-1}, and c_f = 260 km s^{-1} in maximum within highly compressed region.

3.2. Case C_2

[11] In Case C_2, an earlier shock emergence (t_{s0} = 10 hours) allows the incidental shock to ultimately penetrate the MC body within the solar-terrestrial heliospheric range. Only the evolution of v_r is given in Figure 2 to show the concerned MC-shock complex structure. Though an MC generally behaves like a rigid body with a little elasticity, magnetic field lines of the simulated MC appear to be too vulnerable to be easily deformed in the face of an overwhelming shock. The shock is radially emitted with the strongest intensity at front nose. Hence shock front behaves as an oblique curve relative to heliospheric equator due to the propagation speed difference from shock nose to edge flank. The MC is highly compressed by the shock along its normal. The shock front looks like a smooth arc in MC medium. As it propagates gradually into the preceding MC body, the most violent interaction is transferred sideways (heliolatitudinally in the present study). Owing to net shock-input angular momentum

Figure 1. The evolution of shock overtaking magnetic clouds (MC) for Case B_2, with (a)–(c) magnetic field magnitude B, (d)–(f) radial flow speed v_r, and (g)–(i) radial characteristic speed of fast mode c_f. Below each image are two additional radial profiles along Lat. = 0° and 4.5°S. Note that the radial profile of B is plotted by subtracting initial ambient value $B|_{t=0}$. The white solid line in each image denotes the MC boundary. Solid and dashed lines at each profile denote MC core and boundary.

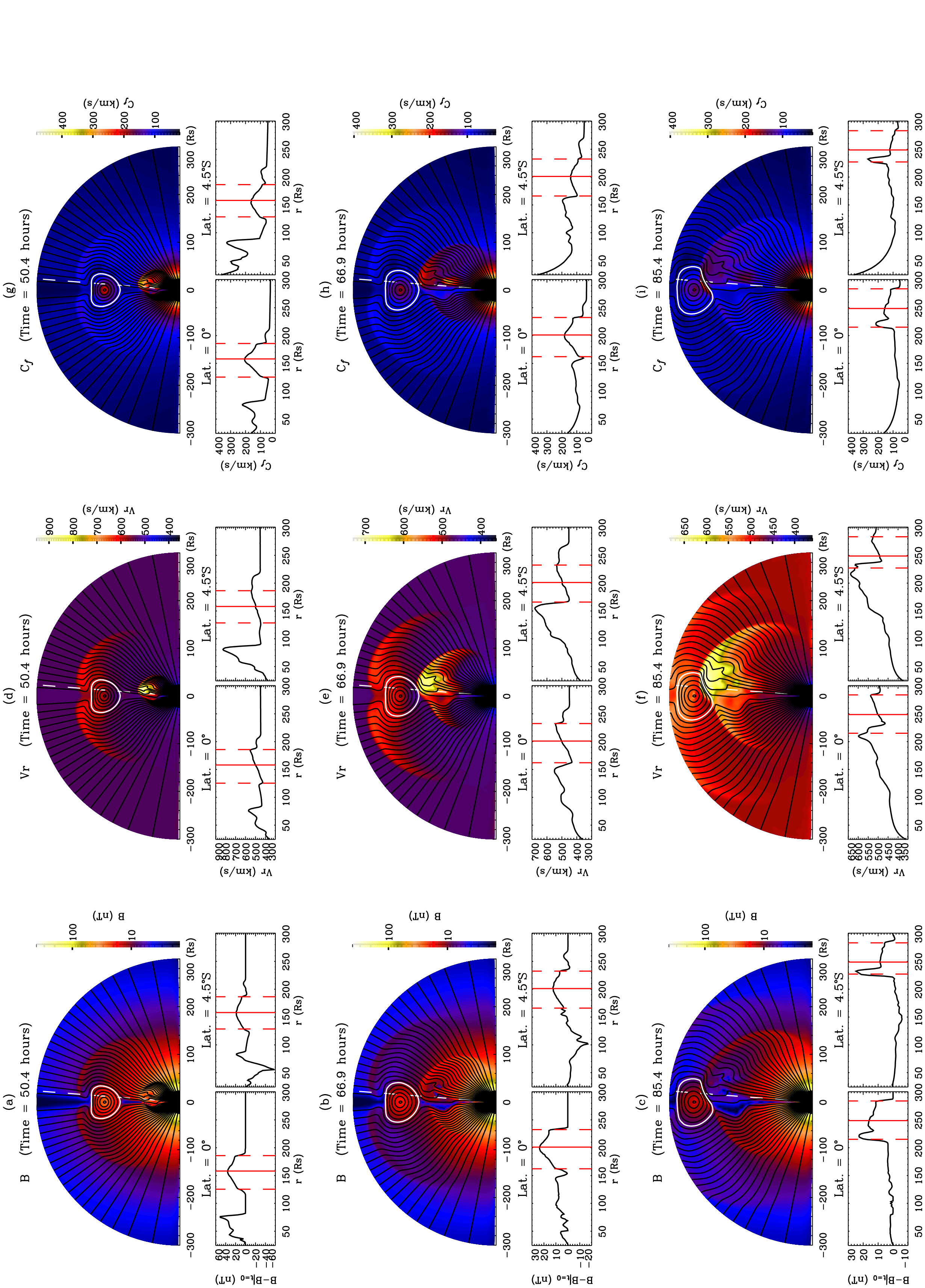
B (a) (Time = 50.4 hours)
B (b) (Time = 66.9 hours)
B (c) (Time = 85.4 hours)
Vr (d) (Time = 50.4 hours)
Vr (e) (Time = 66.9 hours)
Vr (f) (Time = 85.4 hours)
C_f (g) (Time = 50.4 hours)
C_f (h) (Time = 66.9 hours)
C_f (i) (Time = 85.4 hours)
B (nT)
Vr (km/s)
C_f (km/s)
Lat. = 0°
Lat. = 4.5°S
r (Rs)
(Rs)
$B-B|_{t=0}$ (nT)

Figure 1

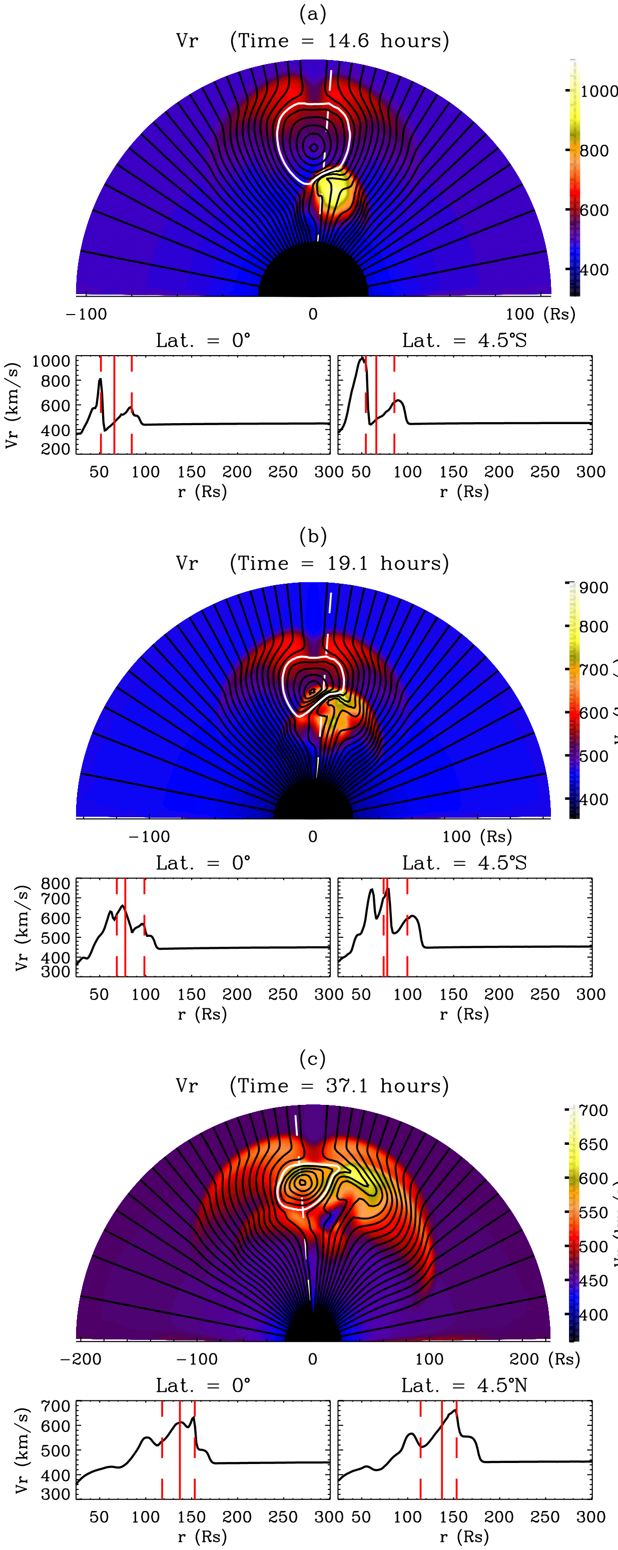

Figure 2. The evolution of shock overtaking MC for Case C_2 with radial flow speed v_r. Only part of domain is adaptively plotted to highlight MC.

during MC-shock OC, the MC core starts to deflect away from initial shock orientation when the shock enters MC core, as seen in the contrast of Figures 2b and 2c. The overall MC body is also deflected to the north. The global MC body deflection is quantified by the deflection angle of its core. Once the shock completely penetrates the MC, the grip of shock force on the MC is substantially relaxed, and the MC is restored to the roughly ellipse morphology by its field line elasticity. Meanwhile, the MC loses its angular speed component by the relative difference between the radial ambient flow and the speed's value at the MC boundary and, then propagates radially along the deflected angle. The incidental shock is also simultaneously deviated with its aphelion in the opposite direction, until it finally merges with the MC-driven shock into a compound one. The bend of interplanetary magnetic field (IMF) lines is obvious near the south of MC boundary, seen from Figure 2c.

[12] Figure 3 shows the comparison among Cases A, C_1, and C_2 about time-dependent parameters: radial distance of

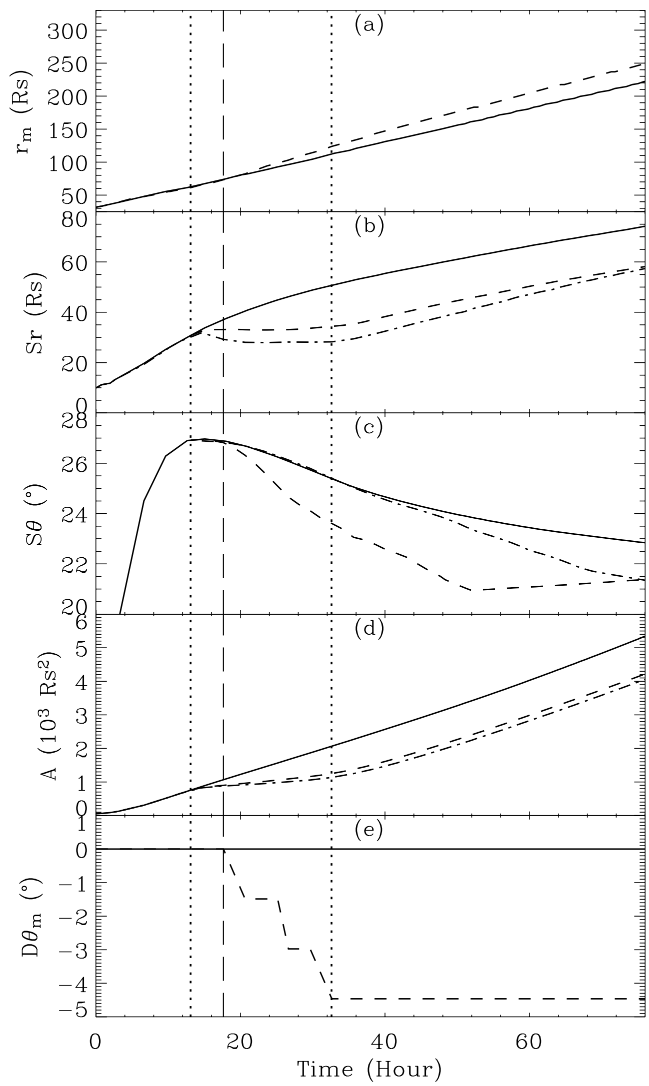

Figure 3. The time dependence of MC parameters: (a) radial distance of MC core r_m, (b) MC radial span Sr, (c) MC angular span $S\theta$, (d) MC cross section area A, and (e) MC core deflection angle $D\theta_m$. The solid, dashed, and dashed-dotted curves denote individual MC event (case A), MC-shock events (cases C_2 and C_1). Three vertical delimiting lines (dotted, dashed, and dotted) from left to right correspond to the occasion of shock encountering MC tail, core, and head, respectively.

MC core r_m (Figure 3a), MC radial span Sr (Figure 3b), MC angular span $S\theta$ (Figure 3c), MC cross section area A (Figure 3d), and MC core deflection angle $D\theta_m$ (Figure 3e), where the solid, dashed and dashed-dotted curves denote Cases A, C_2, and C_1, respectively, and the three vertical delimiting lines (dotted, dashed, and dotted) from left to right correspond to the occasion of shock encountering MC tail, core, and head, respectively. The MC in Case C_2 is largely compressed by the shock, beginning from 13 hours. The dependence of the compression of MC geometry on shock orientation is illustrated by the comparison in Figures 3b–3d. Sr is larger while $S\theta$ is smaller for Case C_2 in Group OC. Though $S\theta$ is little affected in Case C_1 when shock front is in MC body (13 hours $< t <$ 33 hours), it is significantly narrowed in Case C_2. And the MC cross section area A in Case C_2, which represents the overall influence of shock compression due to integration of factor Sr and $S\theta$, is a bit larger than that in Case C_1. Starting from being encountered by the following shock, MC core deflects up to $-4.5°$ until shock front reaches MC head, as seen in Figure 3e. Though total deflection angle of MC core ($-4.5°$) amounts to three computational grids of latitudinal spacing 1.5°, MC deflection, we think, is indeed physical solution. Owing to rough subcell resolution in numerical computation, MC core deflection behaves as a false discrete quantum-like transition instead of a realistic smooth one. However, it does not distort the fundamental physical characteristics in numerical simulation.

3.3. Multicases Comparison

[13] The propagation of MC-shock structure toward the Earth can be detected by L1-orbiting spacecraft, which perform the sentinel duty in space weather alarm system. The montage of the evolution of MC-shock compound at L1 under three typical circumstances is visualized in Figure 4, where Figures 4a–4c correspond to Case R_1 from Group DC and Cases Q_2 and R_2 from Group OC. Though the farthest radial distances of shock front in the north and south of the equator are almost identical in Cases R_1 and Q_2, the shock intensity in the south in Case Q_2 is apparently stronger than its north counterpart. With a smaller emergence interval, the shock in Case R_2 merges completely with the MC-driven shock into a compound one and moves faster in the south by contrast of Figures 4b and 4c. Moreover, the asymmetry of compound shock front with respect to heliospheric equator occurs when the shock erupts sideways relative to the MC propagation. The final MC propagation is slightly deviated from heliospheric equator to northern 4.5° after being ultimately penetrated by the shock, as seen from Figures 4b and 4c. The succedent high-speed flow right after the inner boundary of preceding MC in Group DC, mentioned in paper 1, does not exist in corresponding Group OC, which can be seen from contrast between Figures 4a, 4b, and 4c. The shock front with $\theta_{sc} \neq 0°$ has the oblique normal relative to the preceding MC propagation, so the disturbance of speed enhancement downstream of shock front in Group OC can completely bypass or penetrate the obstacle of MC body and merge with the MC-driven shock.

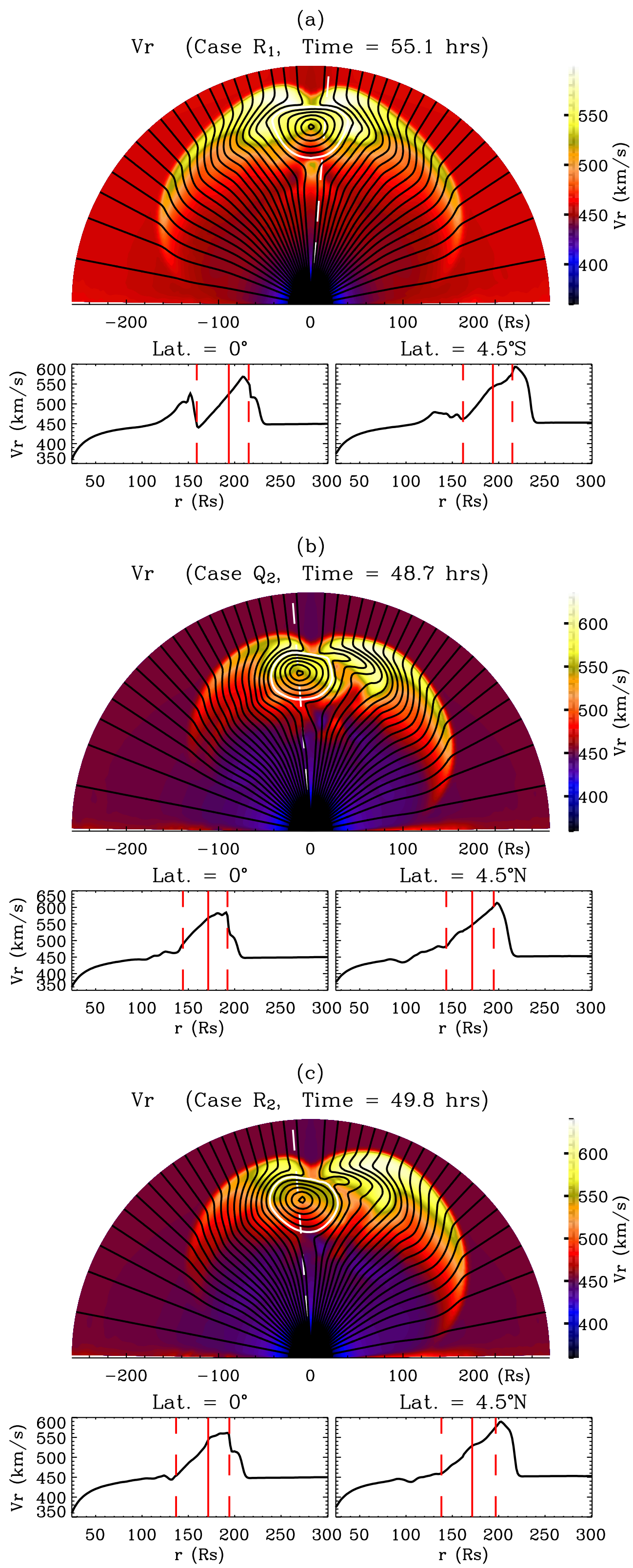

Figure 4. The montage of radial flow speed v_r for the evolution of MC-shock compound at L1 under three conditions.

4. Geoeffectiveness Studies

[14] The southward magnetic flux within the MC is located in its rear part. The geomagnetic effect of simulated B_s event

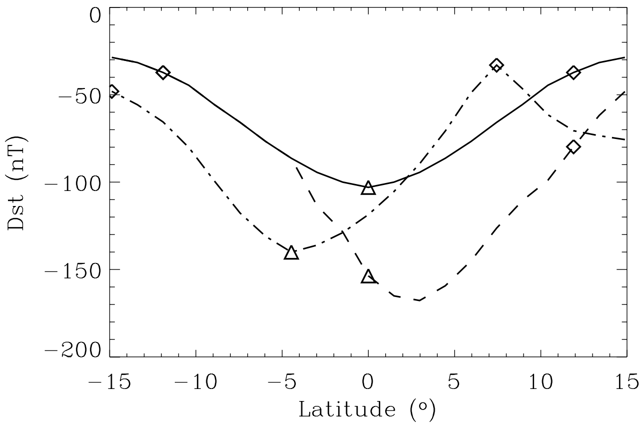

Figure 5. The comparison of latitudinal distribution of *Dst* index among individual MC event (Case A) and MC-shock events (Cases B_2 and C_2). The solid, dashed, and dashed-dotted lines denote Case A, B_2, and C_2, respectively, with the mark Δ, $\diamond$ for the passage of MC core and boundary. The positive and negative latitude are referred to southern and northern semiheliosphere.

is quantified by *Dst* index. The in situ measurements by a hypothetic spacecraft at L1 are input to Burton formula [*Burton et al.*, 1975] to calculate *Dst*, as applied by *Wang et al.* [2003c] and *Xiong et al.* [2006].

[15] Near-HCS latitudinal dependence of *Dst* index in Cases A, B_2, and C_2 is plotted in Figure 5. The positive and negative latitudes are referred to southern and northern semiheliosphere. With the MC core marked by Δ and MC boundary by $\diamond$, the solid, dashed, and dashed-dotted lines denote Cases A, B_2, and C_2, respectively. Geomagnetic storm has been obviously aggravated by shock overtaking MC. The minimum *Dst* is found to be −103 nT, −168 nT, and −140 nT in Cases A, B_2, and C_2, respectively. Cases B_2 and C_2 are discussed one by one against Case A. First, geomagnetic storm in Case A is largely enhanced in Case B_2 within the latitudinal span influenced by the shock. The minimum *Dst* occurs at 3° rather than 0° (the latitude of MC core passage) because the former undergoes more violent compression. The geoeffectiveness remain unchanged within Lat. < −5°. The asymmetry of shock propagation with respect to heliospheric equator leads to subsequent asymmetry of geoeffectiveness of the MC-shock compound. Second, in Case C_2 the concave of the latitudinal distribution of *Dst* is shifted 4.5° to the north. The MC deflection is caused by "noncentral" shock penetrating MC body, as interpreted in section 3.2. As a result, the southward passing magnetic flux decreases due to the northward deflection of MC, and the IMF bend south of the equator due to shock passage, seen from Figure 2c, which are responsible for the increased and decreased *Dst* in 2.3° < Lat. < 9.4° and 9.4° < Lat. < 15°, respectively, comparing with Case A. Therefore as shock front propagates from the south (Case B_2) to the north (Case C_2) in MC medium, the latitude of minimum *Dst* consequently moves in the same direction.

[16] All MC-shock interaction cases of Group OC are integrated to study further the dependence of *Dst* index on the penetration depth d_{Dst} of shock overtaking MC. Here d_{Dst} is defined as the radial distance between shock front and MC inner boundary along Sun-MC core. Three in situ observations in time sequence at L1 along heliospheric equator and ±4.5° aside are synthetically analyzed in Figure 6, where the three vertical delimiting lines (dotted, dashed, and dotted) from left to right correspond to the cases of shock encoun-

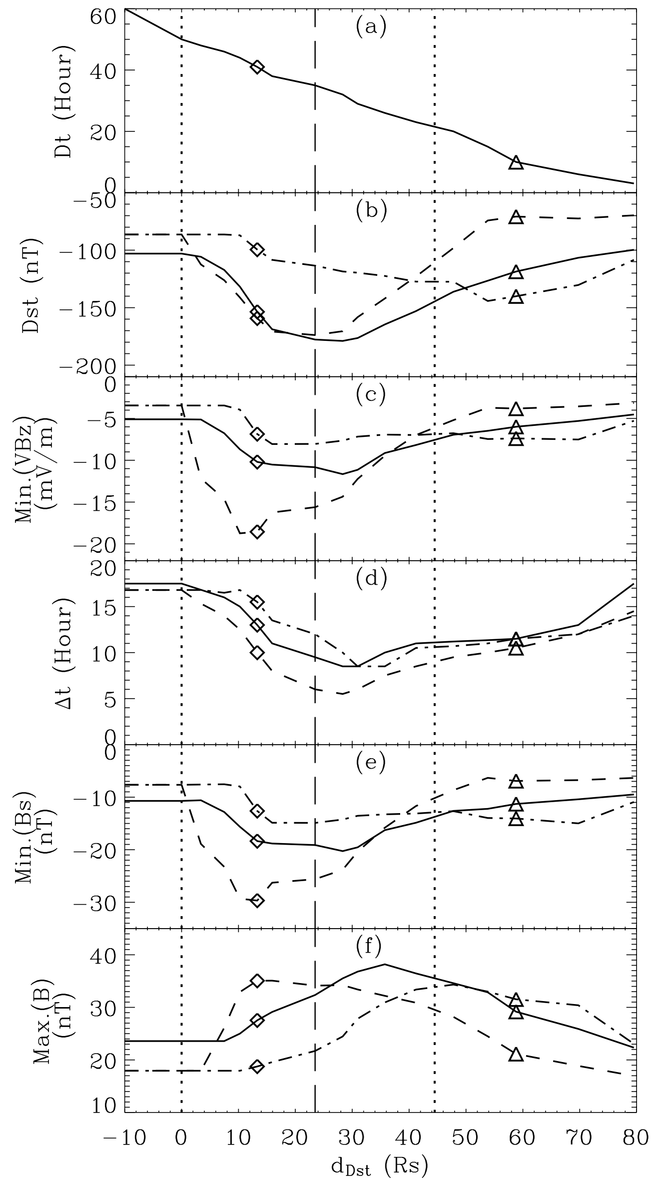

Figure 6. The parameter variances of MC-related geoeffectiveness as a function of d_{Dst} in Group OC. Here d_{Dst} refers to radial distance between shock front and MC inner boundary along Sun-MC core. From left to right, three vertical lines (dotted, dashed, dotted) denote the occasions of shock just reaching MC tail, core, and front at L1, respectively. The mark $\diamond$ and Δ denote corresponding results of Cases B_2 and C_2. (a) *Dt*, MC-shock emergence interval, (b) *Dst* index, (c) Min. (VB_z), the minimum of dawn-dusk electric field VB_z, (d) Δt, the interval between the commencement of $VB_z < -0.5$ mV/m and the corresponding *Dst* minimum, (e) Min.(*Bs*), the minimum of southward magnetic component, and (f) Max.(*B*), the maximum of magnetic magnitude. Solid, dashed and dashed-dotted lines in Figures 6b to 6f correspond to observations along Lat. = 0°, 4.5°S and 4.5°N, respectively.

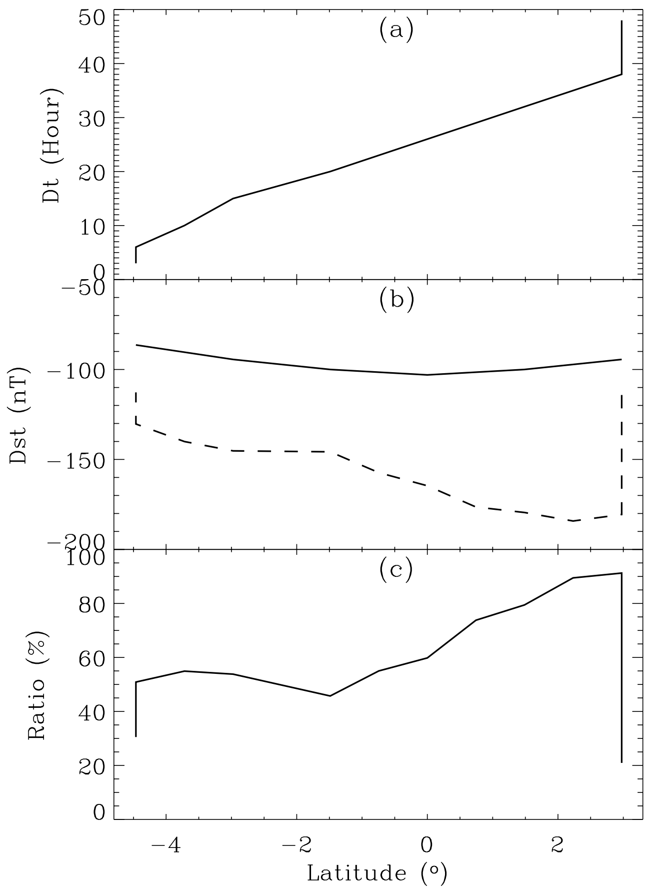

Figure 7. (a–b) The response of the latitude of maximum geoeffectiveness and accompanying *Dst* (dashed line) as the change of MC-shock interval *Dt* in Group OC. The latitudinal distribution of individual MC event (Case A) is denoted in solid line of Figure 7b as background. (c) The relative ratio of geoeffectiveness enhancement by the shock is derived from two curves difference of Figure 7b.

tering the tail, the core and the front of MC at L1, respectively. From top to bottom are plotted MC-shock emergence interval, noted by *Dt* (Figure 6a), the *Dst* index (Figure 6b), the minimum of dawn-dusk electric field VB_z, noted by Min.(VB_z) (Figure 6c), the interval between the commencement of $VB_z < -0.5$ mV/m and the corresponding *Dst* minimum, noted by Δt (Figure 6d), the minimum of southward magnetic component B_s, noted by Min.(B_s) (Figure 6e), and the maximum of magnetic field magnitude Max.(B) (Figure 6f), respectively. The solid, dashed and dashed-dotted lines in Figures 6b–6f correspond to the observations at Lat. = 0°, 4.5°S and 4.5°N, respectively. The separate MC and shock events are coupled together when $Dt < 50$ hours. The shock penetrates into the preceding MC more deeply with shorter *Dt*. Min.(B_s) and Min.(VB_z) decline dramatically along Lat. = 4.5°S as d_{Dst} increases from 0 to $10R_s$, because the first tangent point between MC boundary and shock front is very near 4.5°S. *Dst* decreases monotonically within $0R_s < d_{Dst} < 23.5R_s$ until shock front reaches MC core. Once the shock front exceeds the MC core ($d_{Dst} > 23.5R_s$), the latter begins to deflect northward. Moreover, when $d_{Dst} > 23.5R_s$, the greatest compression region by the shock front is within the MC anterior part or the MC-driven sheath, where magnetic field is northward and hence contributes little to geoeffectiveness. So the mitigated geoeffectiveness along 0°, 4.5°S and aggravated geoeffectiveness along 4.5°N coexist, as seen from $23.5R_s < d_{Dst} < 44.5R_s$ in Figure 6b.

[17] On the basis of the analyses of Figures 5 and 6, MC deflection by MC-shock OC plays a crucial role in geomagnetic storms. The minimum *Dst* and its corresponding latitude among *Dst* latitudinal distribution for every case of Group OC are assembled in Figure 7. With a given *Dt*, there exists a latitude where geoeffectiveness reaches its maximum (Figure 7a). This specific *Dst* value is plotted as dashed line in Figure 7b. The latitudinal distribution of individual MC event (Case A), serving as a background in contrast, is also plotted as solid line in Figure 7b. The relative ratio of geoeffectiveness enhancement by the shock is presented in Figure 7c to quantify two curves difference in Figure 7b. As *Dt* decreases from 48 hours to 3 hours, the latitude of maximum geoeffectiveness firstly remains constant with decreased *Dst* from −115 nT to −180 nT, enhanced ratio from 20% to 91%, then monotonically changes from 3° to −4.5° with gradually subdued geoeffectiveness, finally remains constant again with further increased *Dst* from −130 nT to −115 nT, decreased ratio from 50% to 30%. The minimum *Dst* (−185 nT) occurs at 2.3° when the shock front enters MC core right at 1 AU. In contrast with paper 1, the maximum geoeffectiveness of MC-shock interaction in Group DC is the same as that in Group OC despite occurrence at different heliolatitudes.

5. MC and Shock Deflections

[18] IP MC deflection mentioned in section 3.2 is a key parameter for solar-terrestrial transportation process, because it concerns the preexisting condition of geomagnetic storms, whether an MC could encounter the Earth. In order to explore reliance of MC core deflection angle on shock orientation and intensity, the results of Groups SOD and SID are illustrated in Figure 8. Because MC core continuously deflects on the condition of shock front being in MC medium, seen from Figure 3e, all t_{s0} in Groups SOD and SID are chosen to be 10 hours to have MC completely penetrated for obtaining final invariant angular displacement of MC core $D\theta_m$. *Dst* in Figure 8 refers to the geoeffectiveness at certain latitude of passage of deflected MC core. First, for Group SOD with different θ_{sc}, two factors affect $D\theta_m$: (1) $\theta_{sc} \neq 0$ is a premise of MC core deflection; $D\theta_m = 0$ corresponds to $\theta_{sc} = 0$. (2) As θ_{sc} increases, shock flank section encountered by MC body is further away from shock nose and hence weaker. The absolute value of deflection angle tends to be smaller due to the weakening of MC-shock collision. The maximum deflection of MC core ($D\theta_m = -4.5°$) occurs at certain θ_{sc} ($10° < \theta_{sc} < 15°$). Meanwhile, *Dst* increases monotonically as a function of θ_{sc}, up to the value of corresponding individual MC event. Second, for Group SID with different v_s, both $D\theta_m$ and *Dst* decrease steadily as v_s increases. Moreover, the slopes of two curves in Figures 8c and 8d decrease steadily, very abrupt when $v_s = 1000$ km/s and nearly horizontal when $v_s \geq 3000$ km/s. This saturation effect on $D\theta_m$ and *Dst* is caused by the concurring deflection of shock aphelion opposite to that of MC core mentioned in section 3.2. So the divergent trend of deflection angle

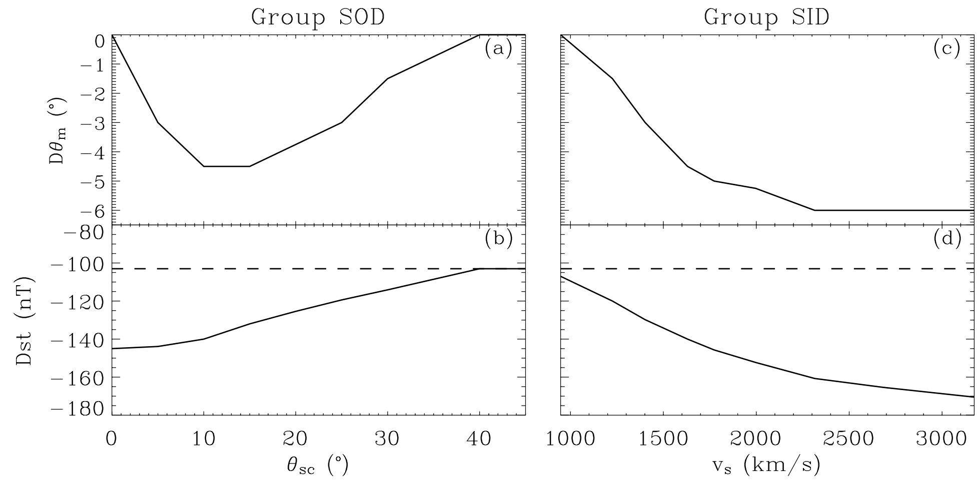

Figure 8. (a–d) The dependence of MC core deflection angle $D\theta_m$ and *Dst* at the specific latitude accompanying MC core passage, on shock eruption orientation θ_{sc} (Group SOD) and speed v_s (Group SID). The horizontal dashed lines in Figures 8b and 8d denote corresponding *Dst* of individual MC event (Case A).

between the MC body and the shock aphelion counteracts, more or less, the effect of increasing shock speed v_s on MC-shock collision.

[19] The finding of MC deflection due to interaction with a shock is further discussed through comparison with other relevant models. (1) *Vandas et al.* [1996] proposed that an MC deflects during the propagation through IP medium with unipolar IMF. Magnetic reconnection between IMF and inherent MC field across one side of MC boundary causes the angular force unbalance and hence leads to angular deflection. The MC continuously deflects through IP space. The role of magnetic helicity is responsible for deflection mechanism [*Vandas et al.*, 1996]. However, such deflection needs to be verified further, as the reconnection should not be so significant in the IP medium with low β; (2) *Wang et al.* [2004] suggested that CMEs could be deflected as largely as several tens degrees in the propagation under the effects of background solar wind and spiral IMF. CME deflects from its onset until accelerated or decelerated to background solar wind, which is expected to be done within several tens solar radii [*Wang et al.*, 2006b]. It can well interpret the observation fact of east-west asymmetry of solar source distribution of Earth-encountered halo CMEs [*Wang et al.*, 2002b] and why some eastern limb CMEs encountered the Earth [*Zhang et al.*, 2003] and some disk CMEs missed the Earth [e.g., *Schwenn et al.*, 2005; *Wang et al.*, 2006a]; (3) Our model here gives that MC deflection only happens during the process of shock front penetrating MC body. The effect of shock pushing MC aside leads to the deviation of MC by several degrees at the most; (4) We conjecture that interaction between ICMEs may also be a cause of ICME deflection, and the deflection angle could be up to tens degrees, larger than that in 3. The propagation trajectory of CMEs mentioned above is deflected from an initial straight line in the IP medium. Both deflections in 1 and 2 are caused by interaction between ambient solar wind and IP disturbance. In contrary, the deflection in 3 and 4 are ascribed to interaction between different IP disturbances, i.e., the collision between MC-shock or MC-MC. It may expect a significant effect on the possibility of CME hitting the Earth in 1, 2, and 4, whereas the effect in 3 may be negligible because of the small deflection angle.

[20] The deflection of shock aphelion in IP medium is a key factor in the near-Earth prediction of shock arrival time. *Hu* [1998] and *Hu and Jia* [2001] stated that the deflection of shock aphelion results from joint effects of spiral IMF and heterogenous medium consisting of fast and slow solar wind. The deflection is also found here in OC of MC-shock. Starting from shock passage through MC medium, shock aphelion deflects toward the contrary trend of MC deflection until the shock totally merges with the MC-driven shock. The final shock aphelion as well as front morphology are distinct from those of isolated shock event. Both MC and shock undergo significant modification during the process of their collision.

6. Concluding Remarks and Discussions

[21] For further understanding of the IP "shock overtaking MC" events [*Wang et al.*, 2003b; *Berdichevsky et al.*, 2005], the investigation of MC-shock interaction and consequent geoeffectiveness in paper 1 is continued by a 2.5-dimensional ideal MHD numerical model. The simulations find that shock eruption orientation relative to preceding MC propagation plays a crucial role in MC-shock interaction.

[22] First, MC-shock dynamical interaction is modeled. In order to reveal the effect of the shock orientation relative to preceding MC propagation, DC in paper 1 is here modified to be OC for MC-shock interaction under the condition of the same shock speed. The results show that the shock front in MC-shock OC behaves as a smooth arc in MC medium. The cannibalized part of MC is highly compressed by the shock along its normal. As the shock propagates gradually into the preceding MC body, the most violent interaction is transferred sideways (in terms of heliolatitude) with an accompanying significant narrowing of the MC's angular width. The opposite deflections of MC body and incidental shock aphelion concur during the process of shock penetrating MC. MC deflection ends when the shock approaches MC

head; shock deflection stops when the shock completely merges with MC-driven shock. After shock passage the MC is restored to oblate morphology. The high-speed flow right after MC inner boundary mentioned in paper 1 does not exist here on the condition of nonuniform orientation of initial MC and shock eruption.

[23] Second, the geoeffectiveness of MC-shock OC is studied. Geoeffectiveness of an individual MC is largely enhanced by an incidental "noncentral" shock. With the decrease of MC-shock commencement interval, shock front at 1 AU traverses MC body and is responsible for the same change trend of the latitude of the greatest geoeffectiveness of MC-shock compound. Among all cases with penetrating shock at various stages, the maximum geoeffectiveness occurs when the shock enters MC core right at 1 AU. *Wang et al.* [2003c] suggested that the maximum geomagnetic storm be caused by shock penetrating MC at a certain depth, and the stronger the incident shock is, the deeper is the position. On the basis of our numerical model, Wang's conclusion of shock penetration depth regarding the maximum geoeffectiveness [*Wang et al.*, 2003c] may be supplemented that shock position is right at MC core on the condition of very strong shock.

[24] Third, the reliance of MC deflection on shock orientation and intensity is explored. The angular displacements of MC body and shock aphelion are ascribed to MC-shock OC. An appropriate angular difference between the initial eruption of an MC and an overtaking shock leads to the maximum deflection of the MC body. The larger the shock intensity is, the greater is the deflection angle. The interaction of MCs with other disturbances could be a cause of ICME's deflected propagation.

[25] **Acknowledgments.** This work was supported by the National Natural Science Foundation of China (40336052, 40404014, 40525014, and 40574063), the Chinese Academy of Sciences (startup fund), and the National Key Basic Research Special Foundation of China (2006CB806304). M. Xiong was also supported by Innovative Fund of University of Science and Technology of China for Graduate Students (KD2005030).

[26] Zuyin Pu thanks Murray Dryer and another reviewer for their assistance in evaluating this paper.

References

Baker, D. N. (2002), How to cope with space weather, *Science*, *297*, 1486–1487.

Berdichevsky, D. B., I. G. Richardson, R. P. Lepping, and S. F. Martin (2005), On the origin and configuration of the 20 March 2003 interplanetary shock and magnetic cloud at 1 AU, *J. Geophys. Res.*, *110*, A09105, doi:10.1029/2004JA010662.

Burlaga, L. F. (1988), Magnetic clouds and force-free fields with constant alpha, *J. Geophys. Res.*, *93*, 7217–7224.

Burlaga, L. F., E. Sittler, F. Mariani, and R. Schwenn (1981), Magnetic loop behind an interplanetary shock: Voyager, helios, and IMP 8 observations, *J. Geophys. Res.*, *86*, 6673–6684.

Burlaga, L. F., S. P. Plunkett, and O. C. St. Cyr (2002), Successive CMEs and complex ejecta, *J. Geophys. Res.*, *107*(A10), 1266, doi:10.1029/2001JA000255.

Burton, R. K., R. L. McPherron, and C. T. Russell (1975), An empirical relationship between interplanetary conditions and Dst, *J. Geophys. Res.*, *80*, 4204.

Dal Lago, A., et al. (2006), The 17–22 October (1999) solar-interplanetary-geomagnetic event: Very intense geomagnetic storm associated with a pressure balance between interplanetary coronal mass ejection and a high-speed stream, *J. Geophys. Res.*, *111*, A07S14, doi:10.1029/2005JA011394.

Detman, T., Z. Smith, M. Dryer, C. D. Fry, C. N. Arge, and V. Pizzo (2006), A hybrid heliospheric modeling system: Background solar wind, *J. Geophys. Res.*, *111*, A07102, doi:10.1029/2005JA011430.

Dryer, M., C. D. Fry, W. Sun, C. Deehr, Z. Smith, S.-I. Akasofu, and M. D. Andrews (2001), Prediction in real time of the 2000 July 14 heliospheric shock wave and its companions during the "Bastille" epoch, *Sol. Phys.*, *204*, 267–286.

Dryer, M., Z. Smith, C. D. Fry, W. Sun, C. S. Deehr, and S.-I. Akasofu (2004), Real time shock arrival predictions during the "Halloween 2003 epoch", *Space Weather*, *2*, S09001, doi:10.1029/2004SW000087.

Farrugia, C. J., L. F. Burlaga, V. A. Osherovich, I. G. Richardson, M. P. Freeman, R. P. Lepping, and A. J. Lazarus (1993), A study of an expanding interplanetary magnetic cloud and its interaction with the Earth's magnetosphere: The interplanetary aspect, *J. Geophys. Res.*, *98*, 7621–7632.

Fry, C. D., W. Sun, C. S. Deehr, M. Dryer, Z. Smith, S.-I. Akasofu, M. Tokumaru, and M. Kojima (2001), Improvements to the HAF solar wind model for space weather predictions, *J. Geophys. Res.*, *106*, 20,985–21,001.

Fry, C. D., M. Dryer, W. Sun, C. S. Deehr, Z. Smith, T. R. Detman, A. Aran, D. Lario, B. Sanahuja, and S.-I. Akasofu (2005), Key links in space weather: Forecasting solar-generated shocks and proton acceleration, *AIAA. J.*, *43*, 987–993.

Goldstein, H. (1983), On the field configuration in magnetic clouds, in *Solar Wind Five*, edited by M. Neugebauer, *NASA Conf. Publ. 2280*, 731–733.

Gombosi, T. I., D. L. DeZeeuw, C. P. T. Groth, K. G. Powell, C. R. Clauer, and P. Song (2001), From Sun to Earth: Multiscale MHD simulations of space weather, in *Space Weather*, *Geophys. Monogr. Ser.*, vol. 125, edited by P. Song, H. J. Singer, and G. L. Siscoe, pp. 169–176, AGU, Washington, D. C.

Gonzalez, W. D., B. T. Tsurutani, and A. L. C. Gonzalez (1999), Interplanetary origin of geomagnetic storms, *Space Sci. Rev.*, *88*, 529.

Gonzalez-Esparza, A., A. Santillan, and J. Ferrer (2004), A numerical study of the interaction between two ejecta in the interplanetary medium: One- and two-dimensional hydrodynamic simulations, *Ann. Geophys.*, *22*, 3741–3749.

Gosling, J. T. (1990), Coronal mass ejections and magnetic flux ropes in interplanetary space, in *Physics of Magnetic Flux Ropes*, *Geophys. Monogr. Ser.*, vol. 58, edited by C. T. Russell, E. R. Priest, and L. C. Lee, p. 343, AGU, Washington, D. C.

Gosling, J. T., D. J. McComas, J. L. Phillips, and S. J. Bame (1991), Geomagnetic activity associated with earth passage of interplanetary shock disturbances and coronal mass ejections, *J. Geophys. Res.*, *96*, 731.

Groth, C. P. T., D. L. De Zeeuw, T. I. Gombosi, and K. G. Powell (2000), Global three-dimensional MHD simulation of a space weather event: CME formation, interplanetary propagation, and interaction with the magnetosphere, *J. Geophys. Res.*, *105*, 25,053–25,078.

Hidalgo, M. A. (2003), A study of the expansion and distortion of the cross section of magnetic clouds in the interplanetary medium, *J. Geophys. Res.*, *108*(A8), 1320, doi:10.1029/2002JA009818.

Hidalgo, M. A. (2005), Correction to "A study of the expansion and distortion of the cross section of magnetic clouds in the interplanetary medium", *J. Geophys. Res.*, *110*, A03207, doi:10.1029/2004JA010752.

Hu, Y. Q. (1998), Asymmetric propagation of flare-generated shocks in the heliospheric equatorial plane, *J. Geophys. Res.*, *103*, 14,631–14,641.

Hu, Y. Q., and X. Z. Jia (2001), Interplanetary shock interaction with the heliospheric current sheet and its associated structures, *J. Geophys. Res.*, *106*, 29,299–29,304.

Larson, D. E., et al. (1997), Tracing the topology of the October 18–20, 1995, magnetic cloud with $\sim 0.1-10^2$ keV electrons, *Geophys. Res. Lett.*, *24*, 1911–1914.

Lugaz, N., W. B. Manchester IV, and T. I. Gombosi (2005), Numerical simulation of the interaction of two coronal mass ejections from sun to earth, *Astrophys. J.*, *634*, 651–662.

Lundquist, S. (1950), Magnetohydrostatic fields, *Ark. Fys.*, *2*, 361–365.

Manchester, W. B., T. I. Gombosi, I. Roussev, D. L. De Zeeuw, I. V. Sokolov, K. G. Powell, G. Toth, and M. Opher (2004a), Three-dimensional MHD simulation of a flux rope driven CME, *J. Geophys. Res.*, *109*, A01102, doi:10.1029/2002JA009672.

Manchester, W. B., T. I. Gombosi, I. Roussev, A. Ridley, D. L. De Zeeuw, I. V. Sokolov, K. G. Powell, and G. Toth (2004b), Modeling a space weather event from the Sun to the Earth: CME generation and interplanetary propagation, *J. Geophys. Res.*, *109*, A02107, doi:10.1029/2003JA010150.

Odstrcil, D., J. A. Linker, R. Lionello, Z. Mikic, P. Riley, V. J. Pizzo, and J. G. Luhmann (2002), Merging of coronal and heliospheric numerical two-dimensional MHD models, *J. Geophys. Res.*, *107*(A12), 1493, doi:10.1029/2002JA009334.

Odstrcil, D., M. Vandas, V. J. Pizzo, and P. MacNeice (2003), Numerical simulation of interacting magnetic flux ropes, in *Solar Wind 10*, edited by M. Velli, R. Bruno, and F. Malara, *AIP Conf. Proc.*, *679*, 699–702.

Osherovich, V. A., C. J. Farrugia, and L. F. Burlaga (1993a), Nonlinear evolution of magnetic flux ropes: 1. low-beta limit, *J. Geophys. Res.*, *98*, 13,225.

Osherovich, V. A., C. J. Farrugia, and L. F. Burlaga (1993b), Dynamics of aging magnetic clouds, *Adv. Space Res.*, *13*, 57.
Osherovich, V. A., C. J. Farrugia, and L. F. Burlaga (1995), Nonlinear evolution of magnetic flux ropes: 1. Finite-beta plasma, *J. Geophys. Res.*, *100*, 12,307.
Owens, M. J., V. J. Merkin, and P. Riley (2006), A kinematically distorted flux rope model for magnetic clouds, *J. Geophys. Res.*, *111*, A03104, doi:10.1029/2005JA011460.
Parker, E. N. (1963), *Interplanetary Dynamical Process*, Wiley-Interscience, New York.
Richardson, I. G., and H. V. Cane (2004), The fraction of interplanetary coronal mass ejections that are magnetic clouds: Evidence for a solar cycle variation, *Geophys. Res. Lett.*, *31*, L18804, doi:10.1029/2004GL020958.
Richardson, I. G., and H. V. Cane (2005), A survey of interplanetary coronal mass ejections in the near-Earth solar wind during 1996–2005, in *Solar Wind 11*, edited by B. Fleck and T. H. Zurbuchen, *Eur. Space Agency Spec. Publ., ESA SP-592*, 154.
Riley, P., and N. U. Crooker (2004), Kinematic treatment of CME evolution in the solar wind, *Astrophys. J.*, *600*, 1035–1042.
Schmidt, J. M., and P. J. Cargill (2003), Magnetic reconnection between a magnetic cloud and the solar wind magnetic field, *J. Geophys. Res.*, *108*(A1), 1023, doi:10.1029/2002JA009325.
Schwenn, R., A. Dal Lago, E. Huttunen, and W. D. Gonzalez (2005), The association of coronal mass ejection with their effects near the earth, *Ann. Geophys.*, *23*, 1033–1059.
Smart, D. F., and M. A. Shea (1985), A simplified model for timing the arrival of solar flare-initiated shocks, *J. Geophys. Res.*, *90*, 183–190.
Smith, Z., and M. Dryer (1990), MHD study of temporal and spatial evolution of simulated interplanetary shocks in the ecliptic plane within 1 AU, *Sol. Phys.*, *129*, 387–405.
Smith, Z., D. Odstrcil, and M. Dryer (1998), A 2.5-dimensional MHD parametric study of interplanetary shock interactions with the heliospheric current sheet/heliospheric plasma sheet, *J. Geophys. Res.*, *103*, 20,581–20,589.
Toth, G., et al. (2005), Space Weather Modeling Framework: A new tool for the space science community, *J. Geophys. Res.*, *110*, A12226, doi:10.1029/2005JA011126.
Tsurutani, B. T., W. D. Gonzalez, F. Tang, S. I. Akasofu, and E. J. Smith (1988), Origin of interplanetary southward magnetic fields responsible for major magnetic storms near solar maximum (1978–1979), *J. Geophys. Res.*, *93*, 8519.
Vandas, M., S. Fischer, M. Dryer, Z. Smith, and T. Detman (1995), Simulation of magnetic cloud propagation in the inner heliosphere in two dimensions: 1. A loop perpendicular to the ecliptic plane, *J. Geophys. Res.*, *100*, 12,285–12,292.
Vandas, M., S. Fischer, M. Dryer, Z. Smith, and T. Detman (1996), Simulation of magnetic cloud propagation in the inner heliosphere in two dimensions: 2. A loop parallel to the ecliptic plane and the role of helicity, *J. Geophys. Res.*, *101*, 2505–2510.
Vandas, M., S. Fischer, M. Dryer, Z. Smith, T. Detman, and A. Geranios (1997), MHD simulation of an interaction of a shock wave with a magnetic cloud, *J. Geophys. Res.*, *102*, 22,295–22,300.
Vandas, M., D. Odstrcil, and S. Watari (2002), Three-dimensional MHD simulation of a loop-like magnetic cloud in the solar wind, *J. Geophys. Res.*, *107*(A9), 1236, doi:10.1029/2001JA005068.
Wang, Y. M., S. Wang, and P. Z. Ye (2002a), Multiple magnetic clouds in interplanetary space, *Sol. Phys.*, *211*, 333–344.
Wang, Y. M., P. Z. Ye, S. Wang, G. P. Zhou, and J. X. Wang (2002b), A statistical study on the geoeffectiveness of Earth-directed coronal mass ejections from March 1997 to December 2000, *J. Geophys. Res.*, *107*(A11), 1340, doi:10.1029/2002JA009244.
Wang, Y. M., P. Z. Ye, and S. Wang (2003a), Multiple magnetic clouds: Several examples during March–April, 2001, *J. Geophys. Res.*, *108*(A10), 1370, doi:10.1029/2003JA009850.
Wang, Y. M., P. Z. Ye, S. Wang, and X. H. Xue (2003b), An interplanetary cause of large geomagnetic storms: Fast forward shock overtaking preceding magnetic cloud, *Geophys. Res. Lett.*, *30*(13), 1700, doi:10.1029/2002GL016861.
Wang, Y. M., P. Z. Ye, S. Wang, and M. Xiong (2003c), Theoretical analysis on the geoeffectiveness of a shock overtaking a preceding magnetic cloud, *Sol. Phys.*, *216*, 295–310.
Wang, Y. M., C. L. Shen, S. Wang, and P. Z. Ye (2003d), An impirical formula relating the geomagnetic storm's intensity to the interplanetary parameters: $\overline{VB_z}$ and Δt, *Geophys. Res. Lett.*, *30*(20), 2039, doi:10.1029/2003GL017901.
Wang, Y. M., C. L. Shen, S. Wang, and P. Z. Ye (2004), Deflection of coronal mass ejection in the interplanetary medium, *Sol. Phys.*, *222*, 329–343.
Wang, Y. M., H. N. Zheng, S. Wang, and P. Z. Ye (2005), MHD simulation on formation and propagation of multiple magnetic clouds in the heliosphere, *Astron. Astrophys.*, *434*, 309–316.
Wang, Y. M., X. H. Xue, C. L. Shen, P. Z. Ye, S. Wang, and J. Zhang (2006a), Impact of major coronal mass ejections on geo-space during 2005 September 7–13, *Astrophys. J.*, *646*, 625.
Wang, Y. M., M. Xiong, H. N. Zheng, C. L. Shen, X. H. Xue, P. Z. Ye, and S. Wang (2006b), Deflected propagation of CMEs in the interplanetary medium, *36th COSPAR Colloq.*, *PSW1-0036-06*, Beijing, China.
Webb, D. F., T. G. Forbes, H. Aurass, J. Chen, P. Martens, B. Rompolt, V. Rusin, S. F. Martin, and V. Gaizauskas (1994), Material ejection: Report of the flares 22 workshop held at Ottawa, Canada, May 1993, *Sol. Phys.*, *153*, 73.
Wei, F., R. Liu, Q. Fan, and X. Feng (2003), Identification of the magnetic cloud boundary layers, *J. Geophys. Res.*, *108*(A6), 1263, doi:10.1029/2002JA009511.
Wei, F., X. Feng, F. Yang, and D. Zhong (2006), A new non-pressure-balanced structure in interplanetary space: Boundary layers of magnetic clouds, *J. Geophys. Res.*, *111*, A03102, doi:10.1029/2005JA011272.
Xiong, M., H. N. Zheng, Y. M. Wang, and S. Wang (2006), Magnetohydrodynamic simulation of the interaction between interplanetary strong shock and magnetic cloud and its consequent geoeffectiveness, *J. Geophys. Res.*, *111*, A08105, doi:10.1029/2005JA011593.
Zhang, J., K. P. Dere, R. A. Howard, and V. Bothmer (2003), Identification of solar sources of major geomagnetic storms between 1996 and 2000, *Astrophys. J.*, *582*, 520–533.

S. Wang, Y. Wang, M. Xiong, and H. Zheng, CAS Key Laboratory for Basic Plasma Physics, School of Earth and Space Sciences, University of Science and Technology of China, Hefei, Anhui 230026, China. (swan@ustc.edu.cn; ymwang@ustc.edu.cn; mxiong@mail.ustc.edu.cn; hue@ustc.edu.cn)